

Robustness of Humans and Machines on Object Recognition with Extreme Image Transformations

Dakarai Crowder
Northeastern University
crowder.d@northeastern.edu

Girik Malik
Northeastern University
malik.gi@northeastern.edu

Abstract

Recent neural network architectures have claimed to explain data from the human visual cortex. Their demonstrated performance is however still limited by the dependence on exploiting low-level features for solving visual tasks. This strategy limits their performance in case of out-of-distribution/adversarial data. Humans, meanwhile learn abstract concepts and are mostly unaffected by even extreme image distortions. Humans and networks employ strikingly different strategies to solve visual tasks. To probe this, we introduce a novel set of image transforms and evaluate humans and networks on an object recognition task. We found performance for a few common networks quickly decreases while humans are able to recognize objects with a high accuracy.

1. Introduction

Driving in heavy rain, snow, or other adversarial conditions, humans rely on their ability to quickly recognize the vehicle or humans in front based on very few high-level cues. These cues indicate the presence of an "object" instead of trying to accurately predict the object class based on low-level features (vehicle make or color of human's clothes). They use previously learned abstract knowledge of the object and make decisions based on their understanding of how objects interact with the environment. Object recognition is one of the most fundamental problems solved by primates for their everyday functioning and survival. The primate visual system is known to be robust to small perturbations in the scene [14], and uses fairly sophisticated strategies to recognize objects in adversarial conditions with a very high accuracy.

Neural networks largely disregard entity-level recognition and "learn" to recognize objects based on bottom-up cues, like contours, color, textures, etc., that allow them to easily exploit "shortcuts" in input distribution [5]. This in-turn affects the performance of networks when attacked

with adversarial input. To probe the limits of this gap in human and network performance, we introduce novel image transformations that go beyond the currently employed techniques of adversarial attacks. We test the limits to which networks can perform an object recognition task with our image transforms on CIFAR100 [7] dataset. We further test human subjects and networks on an object recognition task with the same image and transform combination, and show humans are more robust in solving the task with much greater accuracy.

Related work Ullman et al. [13] use "minimal recognizable images" to test the limits of network performance on object recognition, and show that networks are susceptible to even minute perturbations at that level. Rusak et al. [11] show adversarially trained object recognition model against locally correlated noise improves performance. By removing texture information and altering silhouette contours, Baker et al. [1] show that networks focus on local shape features.

Contributions: Humans show robustness to extreme image transforms on object recognition tasks.

- We introduce novel image transforms to simulate extreme adversarial attacks
- We present an extensive study of how network performance differs with changes in our transforms
- We probe the limit of robustness between humans and networks on object recognition tasks through our transforms

2. Image Transformations

To test the limits of human and machine vision on object recognition task with distorted image structures, we introduce five novel image transformations (Figure 1).

Grid Shuffle divides the image into blocks of equally sized squares, or rectangles. The divided units are individually shuffled with a specified probability (range: [0.0-1.0]).

Randomized Image shuffle shuffles the pixels within the image based on a specified probability (range: [0.0-1.0]),

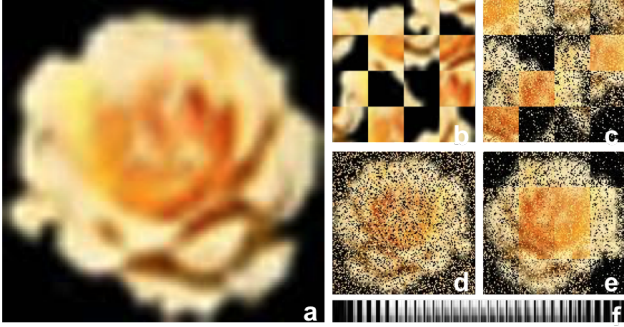


Figure 1. Transforms applied to a CIFAR100 image. (a) non-transformed image, (b) Grid Shuffle with block size 8×8 , (c) Local Grid Shuffle with block size 8×8 and probability 0.5, (d) Randomized Image Shuffle with probability 0.5, (e) Within Grid Shuffle with block size 8×8 and probability 0.5, and (f) Color Flatten.

disregarding any underlying structural properties of the image. For a shuffle probability of 0.5, each pixel’s location has a 50% chance of being shuffled, while a shuffle probability of 1.0 moves every pixel around, with the image looking like random noise.

Within Grid Shuffle divides the image into blocks (similar to Grid Shuffle), but does not shuffle the blocks. Instead, it shuffles the pixels within the blocks with a specified probability. Pixel shuffling within the block is identical to Randomized Image Shuffle, considering each unit in the block to be an individual image.

Local Grid Shuffle is a combination of Within Shuffle and Grid Shuffle. It divides the image into blocks (like Grid Shuffle), shuffles the pixels within the blocks (like Randomized Image Shuffle), and further shuffles the positions of the blocks. It alters both global and local structure of the image.

Color Flatten separates the three RGB channels of the image and flattens the image pixels from 2-dimensional $N \times N$ to three channel separated 1-dimensional vectors of length $N * N$ in row-major order.

3. Model Selection

We selected ResNet50, ResNet101 [6], and VOneResNet50 [4] for our experiments with baseline (no shuffle) and image transformations. VOneResNet50 was selected for its claims of increasing robustness of CNN backbones to adversarial attacks by preprocessing the inputs with a VOneBlock – mathematically parameterized gabor filter bank – inspired by the Linear-Nonlinear-Poisson model of V1. It also had a better V1 explained variance on brain-score [12] benchmark at the time of our experiments. We chose ResNet50 since it formed the CNN backbone of VOneResNet50 and we wanted to test the contribution of non-V1-optimized part of VOneResNet50. We chose ResNet101 for its high average score on brain-score in

terms of popular off-the-shelf models that are widely in use.

4. Experiments

Setup We evaluated ResNet50, ResNet101, and VOneResNet50 on CIFAR100 against baseline images (without transforms), four shuffle transforms, and Color Flatten transform described in 2. We used the default train-test split of 50,000 training images and 10,000 test images from the dataset, distributed over 100 classes. Each image has 3 channels and 32×32 pixels. We did not separate a validation set for network fine-tuning to mimic how humans only see a small subset of objects and then recognize them in the wild, without fine-tuning their internal representations.

Training We trained each model on the baseline and transformed images using the default hyperparameters listed in the repositories of the respective models. For the Grid Shuffle transformation, we used three grid sizes – 4×4 , 8×8 , and 16×16 (dividing image into 4 blocks). For Within Grid Shuffle and Local Grid Shuffle we used a combination of three block sizes (4×4 , 8×8 , and 16×16) with a shuffle probability of 0.5 and 1.0 for each block. For Randomized Image Shuffle we used shuffle probabilities of 0.5 and 1.0. We used a total of 18 different transformations.

In the Color Flatten transform, we separated the image channels and flattened the 2D array to 1D in row-major order. An additional Conv1D layer was added to the networks to process the 1D data, feeding it to the individual networks. All networks were trained end-to-end using only the respective transform (and its hyperparameters), without sharing any hyperparameters across same or different types of transforms.

Human experiments The authors (D.C. and G.M.) also tested themselves on images randomly sampled from the test set of CIFAR100. Images shown to human participants were scaled to 128×128 pixel resolution. The trial screen showed an image and a set of 5 possible object classes that could be present in the image, and asked humans to select the object category closest to the one they see in the image. Each participant was trained on 17 images before the start of the experiment. The training trials consisted of images randomly sampled from CIFAR100 dataset, and then a shuffle transform applied with a unique hyperparameter of grid size and shuffle probability. The hyperparameter combination was not repeated during training (see §S1 for details).

We evaluated humans and networks on 93 trials during testing. Similar to training phase, we showed a single image during a trial, with or without the transforms. The transforms had same hyperparameters as used with networks. Each transform had about 5 different classes of images sampled from CIFAR100, with every transform applied on every image, showing the same transform multiple times, but not with the same image. We additionally asked humans to indicate their level of confidence for their response.

5. Results

Table 1. Test accuracy for models trained on CIFAR100 dataset

Transform	P	Grid Size	Accuracy (in %)		
			ResNet50	ResNet101	VOne
Baseline			47.80	72.10	99.66
Random Shuffle	0.5		36.56	37.53	35.08
	1		18.80	18.79	9.81
Grid Shuffle		4x4	29.35	29.86	16.75
		8x8	35.79	36.69	26.05
		16x16	44.88	46.40	36.29
Within Grid Shuffle	0.5	4x4	44.89	44.86	39.24
		8x8	40.14	40.11	37.47
		16x16	37.91	38.48	36.97
	1	4x4	42.68	42.98	37.70
		8x8	34.73	35.29	31.59
		16x16	25.51	25.89	17.70
Local Grid Shuffle	0.5	4x4	23.94	24.40	18.66
		8x8	26.99	26.80	21.87
		16x16	32.30	32.50	28.02
	1	4x4	23.03	23.42	16.64
		8x8	24.29	24.49	19.17
		16x16	22.99	25.50	16.16
Color Flatten			46.72	47.48	44.22

VOneResNet50 performs the best on baseline (without transforms) CIFAR100 test images, with 99.6% accuracy, followed by ResNet101 and ResNet50 (Table 1). Transforming images significantly reduces performance, with none of the networks being able to reach 50% accuracy. However, ResNet50 and ResNet101 consistently perform better than VOneResNet50 by a large margin. ResNet101 performs better than ResNet50, but the difference is not significant. In case of Randomized Image Shuffle, the accuracy expectedly decreases with an increase in shuffle probability. For Grid Shuffle, the accuracy monotonically increases with an increase in grid size.

Within Grid Shuffle preserves the local structure of the image, adversarially affecting the performance with an increase in grid size and shuffle probability. Smallest grid size is the least affected by increase in shuffle probability. All networks struggle the most on Local Grid Shuffle. Large grid size with low shuffle probability gives a higher accuracy than other variants of grid and shuffle probability, but is overall lower than the other transforms. Flattening the images across color channels gives a higher accuracy across all transforms.

Comparison with Human responses Human subjects performed better than all networks on all but Color Flatten transform (Table S2). Humans had a perfect accuracy on baseline, Randomized Image Shuffle (0.5 shuffle probab-

ity), and 16×16 Grid Shuffle. We ran Ordinary Least Squares regression (OLS) to check if the data from human responses fits the responses from the three networks on the same images shown to the human observers (see Table S1 for comparison of human and network responses on different transforms). Comparing human and network responses for all transforms and their respective hyperparameters, we can reject our null hypothesis that human and machine responses are correlated (Table S3).

We also used OLS on the human and machine responses for individual transforms (Tables S4, S5, S6, S7, S8, S9). For Grid Shuffle, Local Grid Shuffle, Randomized Image Shuffle, and Within Grid Shuffle, we can safely reject the null hypothesis with 99% confidence interval. For baseline and Randomized Image Shuffle, human responses might be correlated with all networks. For Color Flatten, we could only reject the null hypothesis with 95% CI. Few transforms with 16×16 grid might make it easy to understand the basic structure of objects from shape and contours. To test if it aids networks as much as humans, we compared human and network responses only for images that were transformed with a 16×16 grid – namely Grid Shuffle, Within Grid Shuffle and Local Grid Shuffle – with both shuffle probabilities (Table S10). We found that we can reject the null hypothesis, concluding that humans employ different techniques than machines to solve seemingly easy tasks.

6. Discussion and Conclusion

VOneResNet50, ResNet101 and ResNet50 struggle to solve object recognition task on CIFAR100 when trained and tested with our novel transforms. Humans, however, can recognise objects on extreme transforms, implying that humans and networks use very different strategies for object recognition with perturbed images. We show that these differences in strategies are statistically significant.

Unlike initial layers of CNNs that learn edges, contours, and textures, humans rely on an abstract concept of "object" representation and further add individual features linking it with object's category. The abstract concept of object helps humans to learn about the characteristics of the object and link it with the accompanying information about the environment, dimensionality, etc.. This happens at various levels of the human visual system [3]. During object's interaction with the environment, humans treat the object (independent of the class) as a whole individual entity, as opposed to parts of it interacting separately. (The representation of the object being referred to here is atomic in nature. For entities with moving parts, individual parts must be treated as individual objects.)

While CNNs learn representations in a feature specific manner, largely discounting the characteristic properties of the underlying object, humans try to learn the knowledge of features, building on top of objects. We speculate this

might be reflected in our results as well. Networks struggle to link features to an object class when the features are shuffled, but humans’ internal representations are robust to the effects of such distortions, as we show in Table S2. Networks are unable to perform on our easiest transforms with a 16×16 grid, specifically the 16×16 Grid Shuffle – which divides the image into 4 blocks and shuffles them, preserving features closest to the baseline images – demonstrating heavy reliance on features like object shape.

Recent work has shown the ability of CNNs to explain variance in V1, and has gone a step further to create network layers in-line with the variance [4]. Other works have demonstrated learning with noise [2]. These networks perform well on adversarial tasks with controlled attacks. We show how they behave when the control is taken away. We think our work can pave the way for adversarial testing with extreme attacks. We are unsure if CNNs are the right contenders for dealing with such attacks, given the primate visual system has dependency on feedback. Recurrent networks have previously demonstrated good performance [8] on tasks where CNNs struggle [9].

We demonstrate that human visual system employs a more robust strategy to solve the object recognition task, and remains largely unaffected by the seemingly extreme changes in images. Our novel transforms highlight a blind spot for the controlled training of adversarial networks. We hope these transforms can help with development/training of robust architectures simulating tolerance of primate visual system to deal with extreme changes in visual scenes often found in everyday settings.

7. Limitation and Future Work

We used CIFAR100 with 60,000 images distributed over 100 classes. Using a larger dataset could have yielded more stable results. Due to resource limitations, we could collect data from only authors as human subjects. While the network experiments and human data collection were weeks apart, it could still have introduced some bias. We used only 5 unique images across transforms (with its hyperparameters). The tradeoff we faced was between reducing the time spent on human trials to not lose attention v/s using a larger set of images that might have stabilized the results even more. While the classes were unique and the order of presentation was randomly shuffled for each subject, we cannot rule out the possibility of memorization across different hyperparameters of the transformations.

Using coarse and fine labels of CIFAR100, we aim to train these networks on a mix of labels to see if the network learns the representation of an abstract entity like 4-legged animal and could then fine-tune for cat, dog, etc. While some previous work [10] tries to adopt similar approach with human labels, we think the community could benefit with work using extreme transforms.

References

- [1] Nicholas Baker, Hongjing Lu, Gennady Erlikhman, and Philip J Kellman. Deep convolutional networks do not classify based on global object shape. *PLoS computational biology*, 14(12):e1006613, 2018. 1
- [2] Manel Baradad Jurjo, Jonas Wulff, Tongzhou Wang, Phillip Isola, and Antonio Torralba. Learning to see by looking at noise. *Advances in Neural Information Processing Systems*, 34:2556–2569, 2021. 4
- [3] Matteo Carandini et al. Do we know what the early visual system does? *Journal of Neuroscience*, 25(46):10577–10597, 2005. 3
- [4] Joel Dapello, Tiago Marques, Martin Schrimpf, Franziska Geiger, David Cox, and James J DiCarlo. Simulating a primary visual cortex at the front of cnns improves robustness to image perturbations. *Advances in Neural Information Processing Systems*, 33:13073–13087, 2020. 2, 4
- [5] Robert Geirhos et al. Generalisation in humans and deep neural networks. *Advances in neural information processing systems*, 31, 2018. 1
- [6] Kaiming He, Xiangyu Zhang, Shaoqing Ren, and Jian Sun. Deep residual learning for image recognition. In *Proceedings of the IEEE conference on computer vision and pattern recognition*, pages 770–778, 2016. 2
- [7] Alex Krizhevsky, Geoffrey Hinton, et al. Learning multiple layers of features from tiny images. 2009. 1
- [8] Drew Linsley *, Girik Malik *, Junkyung Kim, Lakshmi Narasimhan Govindarajan, Ennio Mingolla †, and Thomas Serre †. Tracking without re-recognition in humans and machines. In *Proceedings of the 35th International Conference on Neural Information Processing Systems*, 2021. 4
- [9] Girik Malik, Drew Linsley, Thomas Serre, and Ennio Mingolla. The challenge of appearance-free object tracking with feedforward neural networks. *CVPR Workshop on Dynamic Neural Networks Meet Computer Vision*, 2021. 4
- [10] Joshua C Peterson, Ruairidh M Battleday, Thomas L Griffiths, and Olga Russakovsky. Human uncertainty makes classification more robust. In *Proceedings of the IEEE/CVF International Conference on Computer Vision*, pages 9617–9626, 2019. 4
- [11] Evgenia Rusak et al. A simple way to make neural networks robust against diverse image corruptions. In *European Conference on Computer Vision*, pages 53–69. Springer, 2020. 1
- [12] Martin Schrimpf et al. Brain-score: Which artificial neural network for object recognition is most brain-like? *bioRxiv preprint*, 2018. 2
- [13] Shimon Ullman, Liav Assif, Ethan Fetaya, and Daniel Harari. Atoms of recognition in human and computer vision. *Proceedings of the National Academy of Sciences*, 113(10):2744–2749, 2016. 1
- [14] Zhenglong Zhou and Chaz Firestone. Humans can decipher adversarial images. *Nature communications*, 10(1):1–9, 2019. 1

Robustness of Humans and Machines on Object Recognition with Extreme Image Transformations – Supplementary Information –

S1. Human Experiments Setup

The authors, D.C and G.M. were the two participants in the study for collecting human responses for the different transformations. The experiment was not time bound and could be completed at participants own pace. The experiment was designed to take an average of 20-25 minutes. We recorded the reaction time for all trials. After every trial, participants were redirected to a screen confirming their submission. They could continue by clicking the "Continue" button or pressing the spacebar. They were automatically redirected from the confirmation screen to the next screen in 3000ms. We also showed a "rest screen" after completion of 10 trials, with a progress bar. The rest screen was shown only during main trials and not during practice trials. The time on rest screen was not recorded.

Experiment design At the beginning of the experiment, the participants were shown an information screen guiding them about the significance of the experiment and what needs to be done. They could then click "Continue", which showed an instruction modal pop-up with instructions about what to do. They could view this instruction modal anytime during the experiment by clicking the button "Instructions" in the top right corner of their screens.

Participants were shown an image (baseline or transformed) along with five object classes from the CIFAR100 labels. They were asked to identify the object in the image and select the option closest to what they thought the object in the image was. They were also asked to rate their level of confidence on a scale of 1 through 5, ranging from least to most confident. They were given a feedback on their response in the form of correct or incorrect during practice trials but not during the main test trials. Each trial screen also had a short excerpt of instructions. Participants were shown a total of 17 practice trials and 88 test trials.

Software setup The experiment used Python Flask for backend scripts and logic, and HTML, Bootstrap CSS framework and JavaScript for frontend. The form submission through keys and automatic redirections were done using jQuery on the user side. The server was run on HP Z200 workstation using 1 Intel(R) Xeon(R) CPU and 16 GB RAM.

CIFAR100 has 3-channel images of 32×32 pixel resolution. For showing to human participants, the images were sampled from test set at the original resolution and then

scaled to 128×128 pixel resolution using linear interpolation, before applying the required transform on them.

S2. Statistical Analysis of Human and Network Data

To test the significance of human responses to the data returned from the network, we used Ordinary Least Squares regression (OLS) to fit human and machine data. We used `statsmodels` library in python for our analysis.

Table S1. Summary table for OLS Linear Probit Models across different transforms

	All data	Baseline	Randomized Image Shuffle	Grid Shuffle	Within Grid Shuffle	Local Grid Shuffle	Color Flatten	All 16 × 16 transforms
Humans (con.)	0.7966*** (0.0422)	1.0000*** (0.2000)	0.7500*** (0.1830)	1.0000*** (0.1024)	0.8667*** (0.0745)	0.7333*** (0.0889)	0.0000 (0.2000)	0.8000*** (0.0856)
VOneResNet50	-0.4492*** (0.0597)	-0.4000 (0.2828)	-0.2500 (0.2588)	-0.7333*** (0.1447)	-0.5667*** (0.1053)	-0.3333*** (0.1257)	0.6000** (0.2828)	-0.5600*** (0.1211)
ResNet101	-0.4576*** (0.0597)	-0.4000 (0.2828)	-0.2500 (0.2588)	-0.7333*** (0.1447)	-0.7000*** (0.1053)	-0.2667** (0.1257)	0.6000** (0.2828)	-0.5200*** (0.1211)
ResNet50	-0.4661*** (0.0597)	-0.2000 (0.2828)	-0.2500 (0.2588)	-0.7333*** (0.1447)	-0.6333*** (0.1053)	-0.3667*** (0.1257)	0.8000** (0.2828)	-0.6000*** (0.1211)

Standard errors in parentheses.

* p<.1, ** p<.05, ***p<.01

Table S2 Model and human accuracy on the same CIFAR100 images

Transform	P	Grid size	Accuracy (in %)			
			ResNet50	ResNet101	VOne	Human
Baseline			80	60	60	100
Randomized Image Shuffle	0.5		50	25	75	100
	1		25	75	20	37.5
Grid Shuffle		4x4	20	40	0	80
		8x8	40	40	40	90
		16x16	20	0	40	100
Within Grid Shuffle	0.5	4x4	40	0	60	90
		8x8	40	20	20	70
		16x16	30	40	20	50
	1	4x4	40	40	40	80
		8x8	20	0	40	60
		16x16	0	0	0	60
Local Grid Shuffle	0.5	4x4	60	40	40	60
		8x8	20	60	40	50
		16x16	20	60	40	70
	1	4x4	40	40	60	50
		8x8	40	40	40	30
		16x16	40	40	20	30
Color Flatten			80	60	60	0

Table S3. OLS for all data (baseline and transforms)

Dep. Variable:	y	R-squared:	0.139			
Model:	OLS	Adj. R-squared:	0.132			
Method:	Least Squares	F-statistic:	19.87			
Date:	Sat, 07 May 2022	Prob (F-statistic):	5.89e-12			
Time:	20:36:26	Log-Likelihood:	-241.54			
No. Observations:	372	AIC:	491.1			
Df Residuals:	368	BIC:	506.8			
Df Model:	3					
	coef	std err	t	P> t 	[0.025	0.975]
Humans	0.7957	0.048	16.478	0.000	0.701	0.891
VOneResNet50	-0.4194	0.068	-6.141	0.000	-0.554	-0.285
ResNet101	-0.4409	0.068	-6.456	0.000	-0.575	-0.307
ResNet50	-0.4301	0.068	-6.298	0.000	-0.564	-0.296
Omnibus:	2791.922	Durbin-Watson:	2.020			
Prob(Omnibus):	0.000	Jarque-Bera (JB):	33.509			
Skew:	0.228	Prob(JB):	5.29e-08			
Kurtosis:	1.602	Cond. No.	4.79			

Table S4. OLS for Baseline

Dep. Variable:	y	R-squared:	0.147			
Model:	OLS	Adj. R-squared:	-0.013			
Method:	Least Squares	F-statistic:	0.9167			
Date:	Sat, 07 May 2022	Prob (F-statistic):	0.455			
Time:	13:36:24	Log-Likelihood:	-10.053			
No. Observations:	20	AIC:	28.11			
Df Residuals:	16	BIC:	32.09			
Df Model:	3					
	coef	std err	t	P> t 	[0.025	0.975]
Humans	1.0000	0.200	5.000	0.000	0.576	1.424
VOneResNet50	-0.4000	0.283	-1.414	0.176	-1.000	0.200
ResNet101	-0.4000	0.283	-1.414	0.176	-1.000	0.200
ResNet50	-0.2000	0.283	-0.707	0.490	-0.800	0.400
Omnibus:	3.241	Durbin-Watson:	2.525			
Prob(Omnibus):	0.198	Jarque-Bera (JB):	2.513			
Skew:	-0.750	Prob(JB):	0.285			
Kurtosis:	2.125	Cond. No.	4.79			

Table S5. OLS for Randomized Image Shuffle

Dep. Variable:	y	R-squared:	0.048			
Model:	OLS	Adj. R-squared:	-0.054			
Method:	Least Squares	F-statistic:	0.4667			
Date:	Sat, 07 May 2022	Prob (F-statistic):	0.708			
Time:	13:45:31	Log-Likelihood:	-22.193			
No. Observations:	32	AIC:	52.39			
Df Residuals:	28	BIC:	58.25			
Df Model:	3					
	coef	std err	t	P> t 	[0.025	0.975]
Humans	0.7500	0.183	4.099	0.000	0.375	1.125
VOneResNet50	-0.2500	0.259	-0.966	0.342	-0.780	0.280
ResNet101	-0.2500	0.259	-0.966	0.342	-0.780	0.280
ResNet50	-0.2500	0.259	-0.966	0.342	-0.780	0.280
Omnibus:	60.696	Durbin-Watson:	2.275			
Prob(Omnibus):	0.000	Jarque-Bera (JB):	4.421			
Skew:	-0.207	Prob(JB):	0.110			
Kurtosis:	1.227	Cond. No.	4.79			

Table S6. OLS for Grid Shuffle (all parameters)

Dep. Variable:	y	R-squared:	0.407			
Model:	OLS	Adj. R-squared:	0.376			
Method:	Least Squares	F-statistic:	12.83			
Date:	Sat, 07 May 2022	Prob (F-statistic):	1.72e-06			
Time:	13:40:05	Log-Likelihood:	-27.549			
No. Observations:	60	AIC:	63.10			
Df Residuals:	56	BIC:	71.47			
Df Model:	3					
	coef	std err	t	P> t 	[0.025	0.975]
Humans	1.0000	0.102	9.770	0.000	0.795	1.205
VOneResNet50	-0.7333	0.145	-5.066	0.000	-1.023	-0.443
ResNet101	-0.7333	0.145	-5.066	0.000	-1.023	-0.443
ResNet50	-0.7333	0.145	-5.066	0.000	-1.023	-0.443
Omnibus:	12.547	Durbin-Watson:	2.281			
Prob(Omnibus):	0.002	Jarque-Bera (JB):	14.931			
Skew:	1.219	Prob(JB):	0.000572			
Kurtosis:	2.818	Cond. No.	4.79			

Table S7. OLS for Within Grid Shuffle

Dep. Variable:	y	R-squared:	0.325
Model:	OLS	Adj. R-squared:	0.308
Method:	Least Squares	F-statistic:	18.62
Date:	Sat, 07 May 2022	Prob (F-statistic):	6.32e-10
Time:	13:46:55	Log-Likelihood:	-60.629
No. Observations:	120	AIC:	129.3
Df Residuals:	116	BIC:	140.4
Df Model:	3		

	coef	std err	t	P> t	[0.025	0.975]
Humans	0.8667	0.074	11.638	0.000	0.719	1.014
VOneResNet50	-0.5667	0.105	-5.381	0.000	-0.775	-0.358
ResNet101	-0.7000	0.105	-6.647	0.000	-0.909	-0.491
ResNet50	-0.6333	0.105	-6.014	0.000	-0.842	-0.425

Omnibus:	9.985	Durbin-Watson:	2.029
Prob(Omnibus):	0.007	Jarque-Bera (JB):	10.557
Skew:	0.726	Prob(JB):	0.00510
Kurtosis:	3.065	Cond. No.	4.79

Table S8. OLS for Local Grid Shuffle

Dep. Variable:	y	R-squared:	0.083
Model:	OLS	Adj. R-squared:	0.059
Method:	Least Squares	F-statistic:	3.503
Date:	Sat, 07 May 2022	Prob (F-statistic):	0.0177
Time:	13:44:13	Log-Likelihood:	-81.874
No. Observations:	120	AIC:	171.7
Df Residuals:	116	BIC:	182.9
Df Model:	3		

	coef	std err	t	P> t	[0.025	0.975]
Humans	0.7333	0.089	8.249	0.000	0.557	0.909
VOneResNet50	-0.3333	0.126	-2.651	0.009	-0.582	-0.084
ResNet101	-0.2667	0.126	-2.121	0.036	-0.516	-0.018
ResNet50	-0.3667	0.126	-2.917	0.004	-0.616	-0.118

Omnibus:	1722.081	Durbin-Watson:	2.362
Prob(Omnibus):	0.000	Jarque-Bera (JB):	13.905
Skew:	0.080	Prob(JB):	0.000956
Kurtosis:	1.340	Cond. No.	4.79

Table S9. OLS for Color Flatten

Dep. Variable:	y	R-squared:	0.360
Model:	OLS	Adj. R-squared:	0.240
Method:	Least Squares	F-statistic:	3.000
Date:	Sat, 07 May 2022	Prob (F-statistic):	0.0615
Time:	13:41:55	Log-Likelihood:	-10.053
No. Observations:	20	AIC:	28.11
Df Residuals:	16	BIC:	32.09
Df Model:	3		

	coef	std err	t	P> t	[0.025	0.975]
Humans	5.392e-16	0.200	2.7e-15	1.000	-0.424	0.424
VOneResNet50	0.6000	0.283	2.121	0.050	0.000	1.200
ResNet101	0.6000	0.283	2.121	0.050	0.000	1.200
ResNet50	0.8000	0.283	2.828	0.012	0.200	1.400

Omnibus:	3.241	Durbin-Watson:	1.900
Prob(Omnibus):	0.198	Jarque-Bera (JB):	2.513
Skew:	-0.750	Prob(JB):	0.285
Kurtosis:	2.125	Cond. No.	4.79

Table S10. OLS for all transforms with 16 × 16 grid

Dep. Variable:	y	R-squared:	0.253
Model:	OLS	Adj. R-squared:	0.230
Method:	Least Squares	F-statistic:	10.84
Date:	Sat, 07 May 2022	Prob (F-statistic):	3.39e-06
Time:	20:32:05	Log-Likelihood:	-55.030
No. Observations:	100	AIC:	118.1
Df Residuals:	96	BIC:	128.5
Df Model:	3		

	coef	std err	t	P> t	[0.025	0.975]
Humans	0.8000	0.086	9.342	0.000	0.630	0.970
VOneResNet50	-0.5600	0.121	-4.624	0.000	-0.800	-0.320
ResNet101	-0.5200	0.121	-4.294	0.000	-0.760	-0.280
ResNet50	-0.6000	0.121	-4.954	0.000	-0.840	-0.360

Omnibus:	6.706	Durbin-Watson:	2.167
Prob(Omnibus):	0.035	Jarque-Bera (JB):	6.940
Skew:	0.621	Prob(JB):	0.0311
Kurtosis:	2.653	Cond. No.	4.79